Inorganic Chemistry
Article
Cite This: Inorg. Chem. XXXX, XXX, XXX−XXX
pubs.acs.org/IC

Mechanistic Features of the Oxidation−Reductive Coupling of Alcohols Catalyzed by Oxo-Vanadium Complexes

Eric Steffensmeier, Matthew T. Swann, and Kenneth M. Nicholas*

Department of Chemistry and Biochemistry, University of Oklahoma, 101 Stephenson Parkway, Norman, Oklahoma 73019, United States

Supporting Information

ABSTRACT: The oxo-vanadium-catalyzed redox disproportionation of activated alcohols (oxidation−reductive coupling, Ox−RC) produces carbonyl compounds and hydrocarbon dimers. A mechanistic study of this novel reaction is reported herein. Following our initial disclosure, new findings include the following: (1) The $[(salimin)VO_2]^-$-catalyzed Ox−RC of Ph_2CHOH in the presence of fluorene affords the products of H-atom abstraction and all possible hydrocarbon dimers. (2) Electronic substituent effects on the relative rates of Ox−RC with respect to 4-X-BnOH reactants and $Bu_4N[(Y\text{-}salimin)VO_2]$ catalysts (**1a−c**) reveal (a) a correlation of the oxidation rate of X-BnOH reactants with the radical σ parameter and (b) correlation of the oxidation rate for $(Y\text{-}salimin)VO_2^-$ with the standard Hammett σ parameter. (3) The ease of electrochemical reduction of **1a−c** is Y = NO_2 > OMe > H. (4) Ambient ^{1}H NMR studies of the interaction of **1** with alcohols suggest only a weak equilibrium association. (5) Density functional theory computational modeling of the Ox−RC reaction supports a ping-pong-type catalytic pathway, beginning with alcohol oxidation by $(salimin)VO_2^-$, preferably by stepwise-H-atom transfer from the alcohol to **1**, affording the carbonyl product and the reduced $(salimin)V(III)(OH)_2^-$. The reduction half-reaction likely begins with condensation of the latter species with R_2CHOH to give the alkoxide complex $(salimin)V(OR)OH^-$; homolysis of the R···OV(III)(salimin) bond affords $(salimin)V(IV)OH(O)^-$ and the R-radical; the latter dimerizes and the former can disproportionate via H-transfer to reform catalyst $(salimin)VO_2^-$ (**1**) and $(salimin)V(OH)_2^-$.

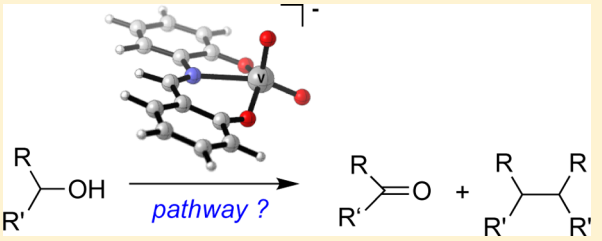

1. INTRODUCTION

The potential value of processes that convert renewable chemical resources into fuels and chemicals has awakened interest in the development of chemical reactions for the refunctionalization of oxygen-rich biomass feedstocks.[1] These incentives have led recently to extensive efforts to discover new and improved methods for polyol dehydration,[2] deoxygenation (DO),[3] and deoxydehydration (DODH, Scheme 1).[4] The

Scheme 1. Hydrodeoxygenation and DODH of Glycols

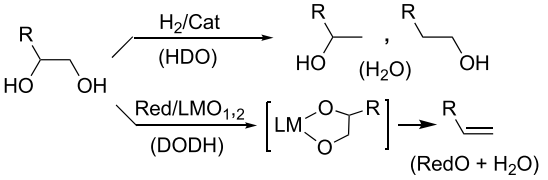

DODH reaction has been developed with oxo-metal catalysts, first of rhenium[5] and then of vanadium[6] and molybdenum,[7] utilizing several reductants, such as phosphines, sulfite, alcohols, hydrogen, and carbon monoxide. Several mechanistic studies point to the common involvement of metalloglycolate intermediates, which, in their reduced state, undergo fragmentation to produce the olefinic products.

We recently discovered a novel reaction for monoalcohol refunctionalization and upgrading, reductive oupling (RC), that is promoted by PPh_3 with $ReO_2I(PPh_3)_2$ as the catalyst (Scheme 2).[8] RC provides a rare catalytic process for C−C

Scheme 2. DO and Reductive Coupling (RC) of Alcohols

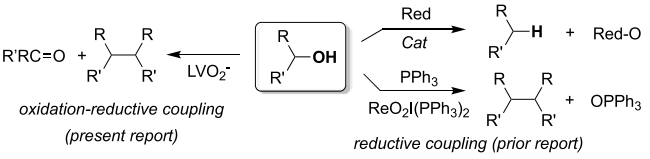

bond formation from alcohols, which in this case doubles their carbon number. The stoichiometric coupling of activated alcohols by reduced Ti-compounds[9] and La/Me_3SiCl[10] has been noted, but to our knowledge, the only catalytic variants known previously were the harsh Cu-catalyzed La/Me_3SiCl[11] coupling and the typically unselective Guerbet reaction.[12] The oxorhenium-catalyzed RC is effective for activated primary and secondary alcohols, especially benzylic and allylic; the tertiary activated alcohol, Ph_3COH, and the α-OH-carbonyl compound, benzil, undergo simple DO. A recently reported

Received: October 18, 2018

DOI: 10.1021/acs.inorgchem.8b02968
Inorg. Chem. XXXX, XXX, XXX−XXX

mechanistic study, including kinetics, stoichiometric reaction studies with spectroscopic detection, and density functional theory (DFT) reaction modeling supports a reaction pathway involving the formation of Re(III)-alkoxide intermediates, via PPh_3-reduction of $ReIO_2(PPh_3)_2$/ROH, and their C−O bond homolysis to generate carbon-free radicals.[13]

In an initial effort to realize a more economical, oxo-vanadium-promoted reductive coupling process, we discovered instead an efficient redox disproportionation of benzylic and allylic alcohols, which results in the coproduction of carbonyl products and primarily reductively coupled hydrocarbon dimers (Scheme 3).[14] Our preliminary observations and

Scheme 3. Oxo-Vanadium-Catalyzed Oxidation−Reductive Coupling (Ox−RC) Reaction

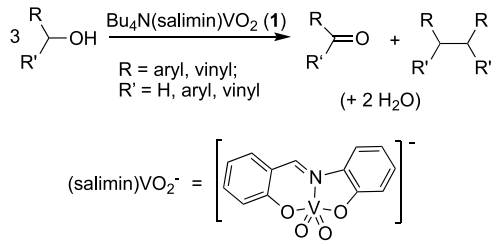

mechanistic probes provided some clues about the reaction pathway and reactive intermediates involved, but were not definitive. The dimeric hydrocarbon products and the formation of regioisomeric allyl dimers from unsymmetrical allylic alcohols were suggestive of symmetrical or isomerizing reactive intermediates such as C-centered radicals. Time-dependent product analysis showed that the formation of the carbonyl product (oxidation) was initially faster than that of the dimer (reduction). A competitive reactivity experiment with Ph_2CHOH/Ph_2CDOH indicated a $k(H)/k(D)$ = 1.0, showing that C−H bond-breaking is not turnover-limiting. Preliminary DFT calculations supported the viability of a catalytic pathway in which the alcohol is first oxidized by LVO_2^- via LV(OH)−OCHR$_2$ (β-H elimination) and subsequent cleavage of a reduced V-alkoxide species to generate the C-radicals for dimerization and/or H-abstraction. To more fully elucidate the details of the reaction pathway (mechanism) and to identify TOL steps and structure/activity relationships that could lead to improved reaction efficiency and substrate scope, we have conducted a more complete investigation that is reported here.

2. RESULTS AND DISCUSSION

We sought to gain stronger evidence for the intermediacy of C-based free radicals by an H-atom transfer trapping experiment. Thus, heating a 1:1 mixture of benzhydrol and the hydrocarbon fluorene under reductive coupling conditions [10 mol % (Bu_4N)(salimin)VO_2 (**1**), PPh_3, 150 °C] produced a reaction mixture that was determined by ^{1}H NMR and gas chromatography (GC)−mass spectrometry (MS) to consist of diphenylmethane, 1,1,2,2-tetraphenylethane (dimer), fluorene-derived bifluorenyl and the mixed dimer diphenylmethyl-fluorenyl, and a small amount of the oxidation product benzophenone (Scheme 4).

These results are most consistent with the generation of the benzhydryl radical in the LVO_2^-/alcohol reaction, which can either dimerize or H-atom abstract from fluorene to generate the fluorenyl radical (Flu) and diphenylmethane (Scheme 5); the two radicals can either self-couple to produce the homodimers or cross-couple to give fluorenyl-$CHPh_2$.

Scheme 5. Pathway Accounting for the H-Transfer Result of Scheme 4

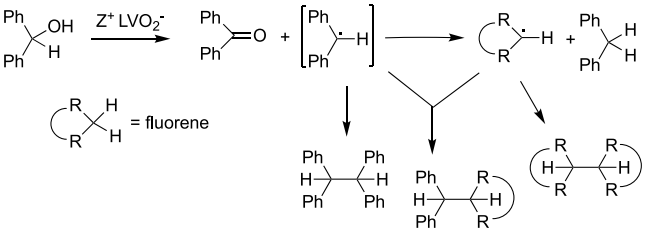

To probe the electronic changes occurring during the catalytic conversion of the alcohol substrates to the oxidation and reduction products, we evaluated the substituent effects on the Ox−RC reaction rates with a set of substituted benzylic alcohols, p-X-$PhCH_2OH$, and a set of ligand-substituted complexes Bu_4N(Y-salimin)VO_2 (**1a−c**). The substituent electronic effects on the substrate alcohol were determined by relative rate competition experiments between $PhCH_2OH$ and p-X-$PhCH_2OH$ (Scheme 6; X = MeO, Me, Cl, CN) under standard reaction conditions [150 °C, benzene, 10 mol % **1a** (Y = H)] proceeding to approximately half conversion. The reaction mixtures were analyzed by GC−MS and ^{1}H NMR to identify and quantify the products and residual reactants and to determine the relative initial rate constants ($k_{rel} = k_Z/k_H$) for disappearance of the alcohols and appearance of aldehydes.[15] It was not possible to unambiguously identify and quantify each of the bibenzyl dimers, so k_{rel} for reductive coupling was not determined. The order of k_{rel} for the appearance of aldehydes (oxidation) shown in Table 1 is Z = CN > OMe > Me > H > Cl.

Hammett-type plots of log k_{rel} for aldehyde formation against the standard σ inductive/resonance parameters[16] failed to give a good linear correlation, with the CN-substituted alcohol being most easily oxidized and a significant outlier. Although the observed nonlinearity could be the result of a change in mechanism [i.e., transition state (TS)] for the p-cyano alcohol, a fair linear correlation for the entire set of alcohols was obtained using Creary's radical σ parameters

Scheme 4. H-Transfer Trapping Reaction between Benzhydrol and Fluorene Promoted by 1

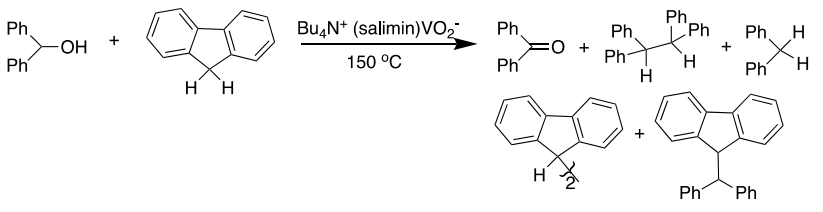

DOI: 10.1021/acs.inorgchem.8b02968
Inorg. Chem. XXXX, XXX, XXX−XXX

Scheme 6. Substrate Competition To Determine Relative Reactivities of Alcohols in Ox−RC

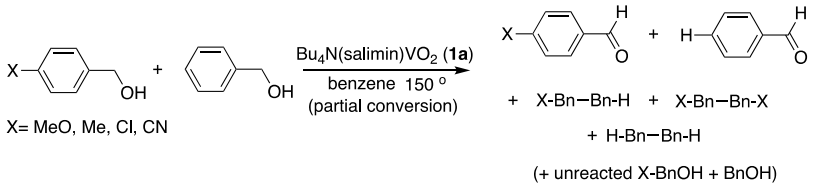

Table 1. Relative Rate Constants for the Formation of Aldehydes in the Catalytic Ox−RC Benzylic Alcohols[a]

4-X-PhCH$_2$OH	σ	k([4-X-PhCHO]/[PhCHO])
OMe	−0.28	2.2
Me	−0.14	1.7
Cl	0.24	0.71
CN	0.70	9.1
H	0.0	1.0

[a]1:1 X-BnOH/H-BnOH, 0.1 cat. **1**, benzene solvent, t = 150 °C; T = 8 h. [4-X-PhCHO]/[PhCHO] determined by H NMR integration.

(Figure 1, R = 0.92),[17] suggesting the development of radical character on the benzylic unit for all of the alcohols in the TS for oxidation to the aldehyde.

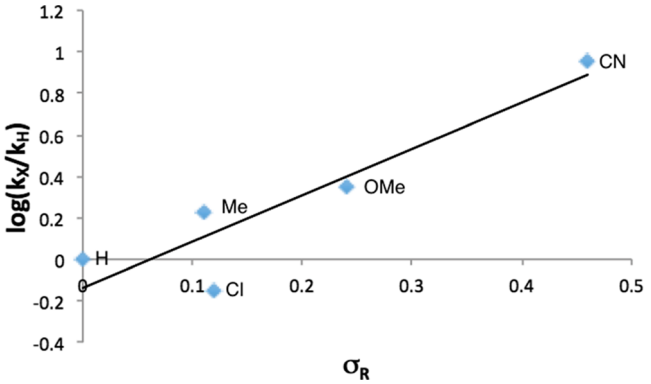

Figure 1. Correlation of relative rates of aldehyde formation from the Ox−RC of 4-X-BnOH catalyzed by Bu$_4$N[(salimin)VO$_2$] (**1a**) with the radical σ parameter, σ_R; R = 0.92 for linear least-squares fit.

Three electronically varied Bu$_4$N$^+$(Y-salimin)VO$_2^-$ complexes were prepared to assess the correlation between the electronic character of the catalyst and the rates of Ox−RC reaction (eq 1), Y = H (**1a**), NO$_2$ (**1b**), and OMe (**1c**). The ligands were prepared by condensation of the respective substituted salicylaldehydes with 2-aminophenol and then converted to the complexes **1a−c** by reaction with Bu$_4$NVO$_3$ in tetrahydrofuran (THF). The compounds **1a−c** were characterized by NMR, IR, electrospray ionization MS (ESI-MS), UV−vis, ^{51}V NMR, and cyclic voltammetry (CV). The spectroscopic characteristics of **1a−c** are unexceptional for LVO$_2$-type species; the ^{1}H NMR spectra are sharp and slightly shifted from the free ligands; IR spectra show V═O ν_{sym} and ν_{asym} between 800 and 900 cm^{-1}; the negative ion ESI-MS show high-intensity molecular ions for the (salimin)VO$_2^-$ ion; and the ^{51}V NMR signals are in the −520 to −530 ppm region, comparable to other five coordinate LVO$_2^-$ complexes.[18]

Reactions of benzhydrol catalyzed by complexes **1a−c** were conducted at T = 150 °C in benzene and were monitored periodically for conversion and product formation by ^{1}H

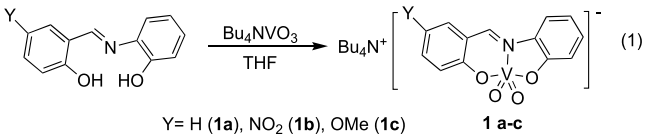

(1)

NMR. Formation of the oxidation product, benzophenone, over time is shown in Figure 2. The concentration versus time

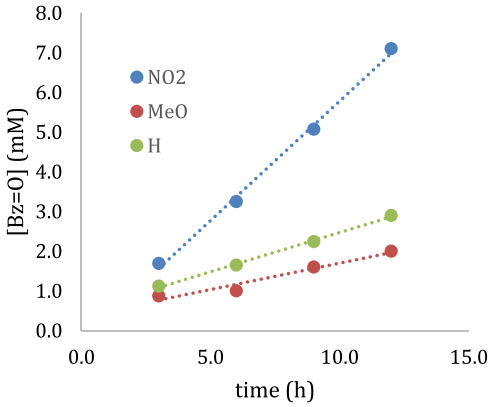

Figure 2. Initial rates of benzophenone formation from the Ox−RC of benzhydrol catalyzedby Bu$_4$N[(Y-salimin)VO$_2$], Y = H (**1a**), NO$_2$ (**1b**), OMe (**1c**).

plots up to approximately 90% conversion were linear, suggestive of a zeroth-order reaction and catalyst saturation kinetics.[19] Slopes of these linear plots (and for dimer formation) were taken as initial rates and when initial concentrations are factored in, give the rate constants for oxidation and reductive coupling summarized in Table 2.

Table 2. Kinetic Data for the Ox−RC of Benzhydrol Catalyzed by (Bu$_4$N)[(Y-Salimin)VO$_2$] (1a−c)[a]

product	Y	rate (M/s)[b]	k_{obs} (s^{-1})[b]
benzophenone	OMe	3.7 × 10^{-8}	1.9 × 10^{-7}
	H	5.5 × 10^{-8}	2.8 × 10^{-7}
	NO$_2$	1.7 × 10^{-7}	8.4 × 10^{-7}
tetraphenylethane	OMe	7.8 × 10^{-8}	3.9 × 10^{-7}
	H	4.5 × 10^{-8}	2.3 × 10^{-7}
	NO$_2$	4.7 × 10^{-8}	2.4 × 10^{-7}

[a]Conditions: initial [Ph$_2$CHOH] = 0.20 M, [**1**] = 0.020 M, benzene, 150 °C. [b]Error estimated at ±10% based on R values from Figure 2 and NMR precision.

The rate constants k_{obs} for oxidation (benzophenone formation) with the L-substituted vanadium complexes follow the order: **1b** (Y = NO$_2$) > **1a** (Y = H) > **1c** (Y = OMe). This sequence parallels the order of the electron-withdrawing ability of the ligand substituent by combined induction/resonance, that is, the more electron-deficient the catalyst, the faster the

DOI: 10.1021/acs.inorgchem.8b02968
Inorg. Chem. XXXX, XXX, XXX−XXX

oxidation. Although the data set is limited, a plot of log k_{rel} for the oxidation process versus the Hammett parameter shows a slope (ρ) of 0.62, indicative of a relatively small negative charge transfer to the Y-salimin ligand of **1a−c** in the TS for oxidation (Figure 3).

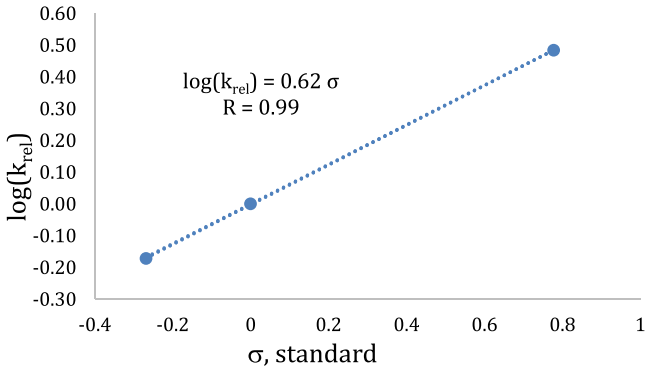

Figure 3. Hammett plot for the rate of production of benzophenone from benzhydrol with catalysts **1a−c** (benzene, T = 150 °C).

The catalyst-dependent rate ordering for reductive coupling (tetraphenylethane formation, Table 2) is: **1c** (OMe) > **1b** (NO_2) ≈ **1a** (H), with a less than a twofold range. That the MeO-substituted complex **1c** is the most active for reductive coupling is consistent with a net greater electron donation via resonance from this substituent, which would facilitate a TS with developing positive charge or electron spin density on the LV unit. However, plots of log k_{rel} for the reductive coupling versus various Hammett σ parameters are nonlinear. This may be the result of counterbalancing substituent effects in the oxidative part of the catalytic cycle. Additional comment is reserved for the Computational Studies section.

3. ELECTROCHEMISTRY

The redox nature of the Ox−RC and the electronic substituent effects noted above implicate the involvement of redox changes on the (salimin)VO_2 species during the catalytic cycle. Because the precatalyst LVO_2^- starts as V(V), one can anticipate a one- or two-electron reduction to V(IV,III) during the catalytic cycle. The facility of such redox changes could be assessed by electrochemical CV experiments. CV studies of the three vanadium complex salts **1a−c** revealed that each undergoes a quasi-reversible reduction process that is characterized by a large peak−peak separation (Figure 4) and is assigned to a one-electron V(V) to V(IV) change. The nonreversibility of the process could be the result of a fast chemical reaction of the reduced LV species or a weakly adsorbed monolayer on the surface of the working electrode, which could be seen visually. For comparison, we thus refer to the values of the $E_{cathode}$ potential (Table 3).

Table 3. Electrochemical Data for Substituted Vanadium Complexes

substituent Y	$E_{cathode}$ (V)	$\lvert E_{anode} - E_{cathode}\rvert$ (V)
NO_2 (**1b**)	0.24	0.22
H (**1a**)	0.11	0.11
OMe (**1c**)	0.17	~0.18

Rather few electrochemical data are available for structurally related LVO_2^- complexes, but the E_{red} potentials determined for **1a−c** are within the broad range of those reported previously.[20] Curiously, both the nitro- and methoxy-substituted complexes **1b,c** are more easily reduced than the parent (Y = H) complex. This is inconsistent with the dominant operation of resonance substituent effects, by which the nitro group is strongly electron-attracting and the methoxy group is electron-donating. However, if one includes only an inductive/field effect as reflected in the σ inductive parameter,[21] a very good linear correlation is found (R = 0.99; see Supporting Information). These results suggest that resonance interactions with the substituent Y are unimportant in determining the ease of forming the one-electron reduced species, (Y-salimin)VO_2^{2-}. Finally, we note that the substituent effects in the CV electron-transfer reduction are different from those in the catalytic alcohol oxidation (which reduces the LVO_2^- species) as illustrated by the nonlinearity of a plot of E_{red} versus k_{rel}. This renders unlikely the involvement of a rate-limiting electron transfer from alcohol to (salimin)VO_2^- in the alcohol oxidation process.

4. NMR STUDY OF Z-SALIMINVO$_2^-$ + ROH INTERACTION

We sought to determine if alcohol/alcoholate complexed intermediates were involved in the (salimin)VO_2-catalyzed Ox−RC by direct spectroscopic analysis of alcohol/(salimin)-

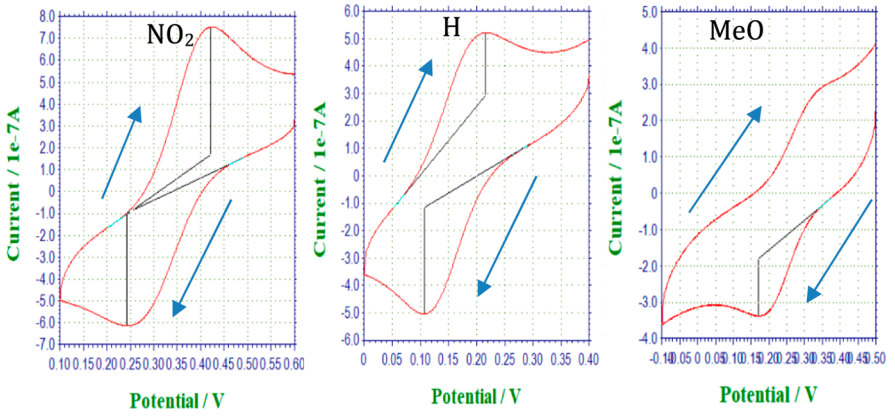

Figure 4. Cyclic voltammagrams for (Bu_4N)(Y-salimin)VO_2; **1b** (Y = NO_2), **1a** (Y = H), and **1c** (Y = OMe) using a Pt working and counter electrode, a Ag/Ag^+ pseudo-reference electrode, (Bu_4N)PF_6 as the electrolyte, and CH_2Cl_2 as the solvent at a scan rate of 100 mV/s.

DOI: 10.1021/acs.inorgchem.8b02968
Inorg. Chem. XXXX, XXX, XXX−XXX

VO_2^- mixtures. When 1−5 equiv of Ph_2CHOH or Me_2CHOH was added to either complex **1a** (Y = H) or **1b** (Y = $-NO_2$) in $CDCl_3$ at room temperature (rt) there was no color change observed over several hours. The ^1H NMR spectra showed only a single set of alcohol- and complex-derived signals, little or unshifted (±0.1 ppm) from those of the alcohol and complex itself; the alcohol R_2CH/OH-coupling disappeared (data in Supporting Information). Standing over 24 h or mild heating to 50 °C over several hours caused no further changes. These observations are inconclusive and could be explained either by there being no significant ambient interaction between the alcohol and complex **1** or alternatively a rapid (on the NMR time-scale), reversible equilibrium between **1**, free alcohol, and an adduct that is little different spectroscopically from the reactants. We note that alcoholate complexes, LV(V)O(OR), are known,[22] but they have not been prepared from $Z^+LVO_2^-$.

5. COMPUTATIONAL STUDIES

We began the computational modeling with an evaluation of the structure and electronic characteristics of the parent (salimin)VO_2^- complex anion of **1**. The structure was optimized with the DFT B3LYP method and 6-31G(d)/LANL2DZ basis sets. The calculated geometry (Figure 5) is

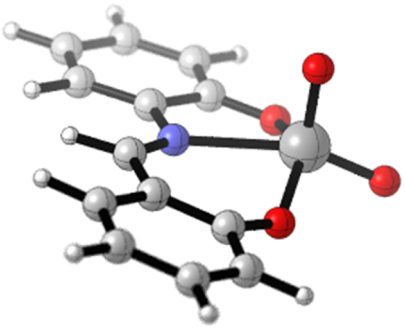

Figure 5. B3LYP-optimized structure of (salimin)VO_2^-; bond lengths and angles are given in the Supporting Information.

that of a distorted square pyramid with the donor O,N,O-atoms of the ligand and one oxo-group in the basal plane and the vanadium atom raised above the plane. The calculated geometry and bond metrics are in good agreement with those of a related (benzosalimin)VO_2^- complex determined by X-ray diffraction;[23] the calculated bond lengths and angles (Supporting Information) are within 2% of the experimental, except for the V−N distance (10%).

The ability of catecholate and related ligands to confer variable redox character on their metal complexes (non-innocence)[24] prompted us to consider whether the complexes **1** exhibited properties indicative of electronic contributions from the resonance forms **B** and **C** (Figure 6) and if this could enhance the reactivity of these complexes as catalysts in alcohol oxidative−reductive coupling. The colors (orange/red) and sharp ^1H NMR signals of **1a−c** indicate that their ground states under ambient conditions are diamagnetic and hence are best described as V(V) species because the formally d^1 V(IV) and d^2 V(III) states, for example, as in contributors **B** and **C**, are typically open shell and paramagnetic. A computational "stable" test of the singlet ground-state optimized structure for **1** revealed no instability, supporting that its ground state is well described as a closed shell singlet. Other proposed indicators of

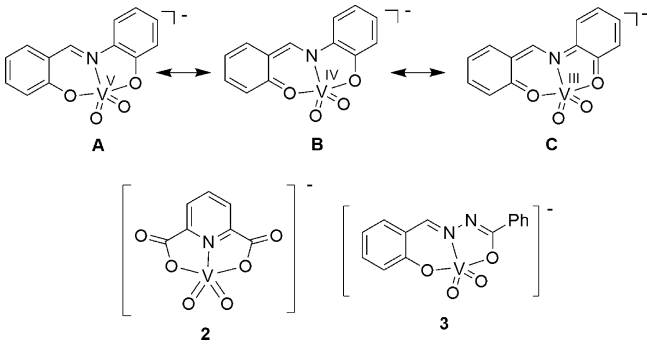

Figure 6. Resonance contributors to (salimin)VO_2^- imparting redox noninnocent ligand character; other O,N,O-donor LVO_2^- compounds, **2** and **3**.

redox noninnocent character include small highest occupied molecular orbital (HOMO)−lowest unoccupied molecular orbital (LUMO) energy gaps and highly shielded ^{51}V NMR chemical shifts.[25] With respect to the latter, the ^{51}V chemical shifts determined for **1a−c** (ca. −530 ppm) are not extraordinary. However, the B3LYP-calculated HOMO−LUMO energy difference in **1** (62 kcal, Figure 7) is

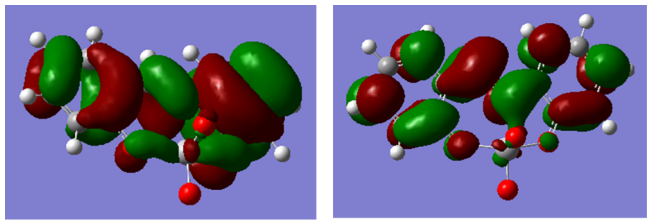

Figure 7. Frontier molecular orbitals calculated for **1a**.

substantially smaller than that of two other known (*O,N,O*-L)VO_2^- compounds, (2,6-pyridinedicarboxylate)VO_2^- (97 kcal) and (salicylhydrazide)VO_2^- (89 kcal), and of the free $saliminH_2$ ligand (94 kcal). This smaller HOMO−LUMO gap could account for the lower energy visible absorptions for **1** (426 nm) relative to **2** and **3**,[26] which would indicate easier access to contributing excited states like **B−D** for **1**. The HOMO, LUMO frontier orbital characteristics are also of interest vis-a-vis other reactivity properties, including the electrochemistry and redox properties of **1**.

The calculated HOMO of **1** (Figure 7) is primarily a ligand-based π-MO with a significant bonding interaction at vanadium using a d_{z^2}-like orbital, but with negligible contribution on the oxido oxygens. The LUMO is almost entirely π-ligand-based. The differing nodal qualities of the HOMO and LUMO of **1a−c** and of the corresponding one-electron reduced species, (salimin)VO_2^{2-} (see Supporting Information), also help to account for the correlation of the reduction potentials of the complexes with the inductive effects of the substituents, that is, ease of reduction of **1a−c**: Z = NO_2 > OMe > H. Significantly, the LUMO of **1a−c** and the singly-occupied molecular orbital of (Y-salimin)VO_2^{2-} both have a node at the C−Y unit, limiting an appreciable Y-salimin π (resonance) interaction.

In evaluating the most probable molecular pathways of the Ox−RC catalysis, we considered that the initial phase of the reaction begins with alcohol oxidation by **1**. This is supported

DOI: 10.1021/acs.inorgchem.8b02968
Inorg. Chem. XXXX, XXX, XXX−XXX

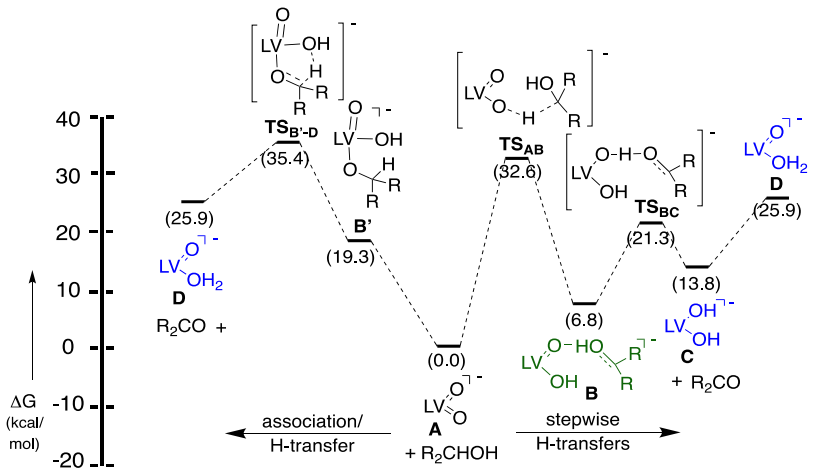

Figure 8. Free-energy reaction profile for alcohol oxidation pathways for the reaction of (salimin)VO_2^- with benzhydrol (L = salimin, R = Ph); association/concerted H-transfer (left) and stepwise H-atom transfers (right).

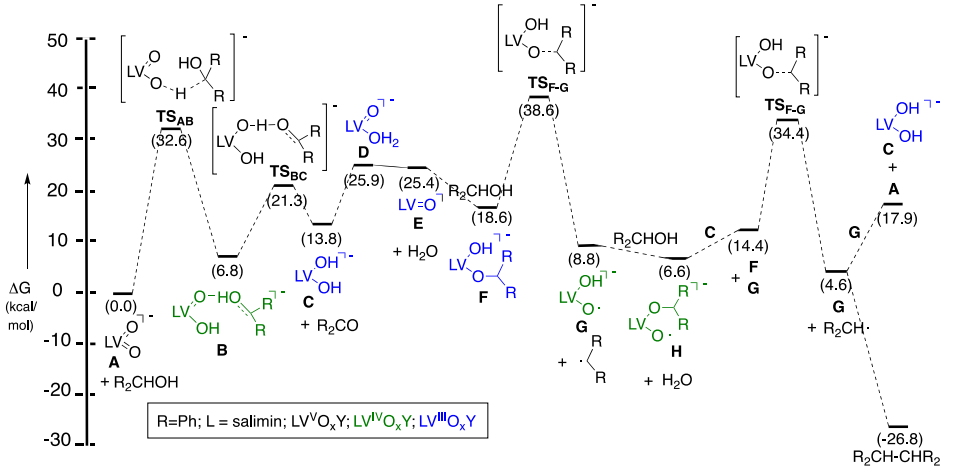

Figure 9. Free-energy reaction profile for the Ox−RC of benzhydrol catalyzed by **1**. Formal oxidation states of vanadium species are color-coded: black = V(V); green = V(IV); blue = V(III).

by our time course reaction monitoring,[11] which showed initially faster formation of benzophenone (oxidized) relative to 1,1,2,2-tetraphenylethane (reduction) and the proven ability of LVO_2 complexes to oxidize activated alcohols.[27] Three different mechanisms were evaluated for alcohol oxidation by **1**: (1) alcohol addition to **1** to give an alkoxo/hydroxo species, that is, $LV(O)OH(OR)^-$, which undergoes concerted *β*-hydride transfer to produce benzophenone, as considered in our initial report; (2) noncoordinative H-transfers from alcohol to complex **1** via either of two sequences, (a) C−H then O−H transfer or (b) O−H then C−H transfer; and (3) concerted O−H/C−H transfer from Ph_2CHOH to LVO_2^-. After structure optimization of intermediates and TSs by the B3LYP method (in vacuo),[28] free energies in solution at rt for all species were obtained by M06[29] single-point calculation with the SMD solvation model (benzene)[30] and zero-point energy and entropic corrections.

The coordinative oxidation pathway involving ROH association with **1** was evaluated in our initial report (pathway 1).[11] Formation of the hydro-alkoxo intermediate **B′** (Figure 8) is calculated to be substantially endoergic (+19.3 kcal), consistent with our NMR nondetection of adduct formation. This contrasts with the behavior of the $ReIO_2(PPh_3)_2$/ROH system in which alcohol/alcoholate adducts form favorably and can be detected at 20 °C.[13] A TS was located for a concerted *β*-H transfer from the alcoholate complex **B′** with a ΔG_{act} value of 16.1 kcal and a total ΔG_{act} value from **1** (**A**) of 35.4 kcal, leading to the V(III)oxo-aquo complex **D**. The ground electronic state for the formally d^2 aquo complex **D** was found to be a triplet ($\Delta E_{triplet/singlet}$ = 13.7 kcal), as is the case for other LV(III) species that we and others have modeled in V-catalyzed DODH[6,14,31] and for most V(III) complexes determined experimentally.[32]

Pathway 2a,b for oxidation via stepwise H-transfers is precedented by the C−H abstraction reactions of d^0-oxometal species with hydrocarbons.[33] H-atom transfer from $Ph_2C\underline{H}OH$ to V═O of **1** (**A** to **B**, Figure 8) was found to be modestly endoergic (6.8 kcal) with a ΔG_{act} value of 32.6 kcal. The lowest energy TS $\mathbf{TS_{A-B}}$ is an open-shell singlet leading to an H-bonded V(IV) intermediate **B**. An initial $Ph_2CHO-\underline{H}$ transfer to **1** (pathway 2b) was also considered (not shown), but it was found to be much more endothermic than the C−H transfer (ΔE_{B3LYP} 31.5 kcal) and is presumed to have a correspondingly higher activation energy. This is likely the result of having to break a stronger O−H versus a C−H bond. From **B**, a subsequent O-to-O H-transfer can occur via $\mathbf{TS_{B-C}}$ with a smaller activation barrier (14.5 kcal) to produce benzophenone and the dihydroxo-V species **C**. The higher total

DOI: 10.1021/acs.inorgchem.8b02968
Inorg. Chem. XXXX, XXX, XXX−XXX

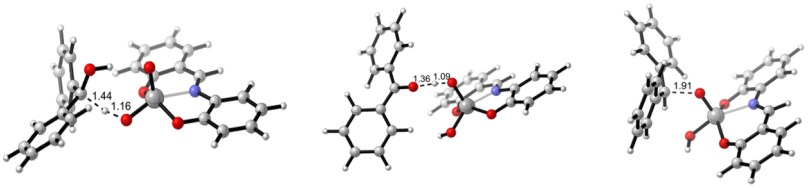

TS_{A-B}		TS_{B-C}		TS_{F-G}	
spin density/charge		spin density/charge		spin density/charge	
V	-0.675/1.09	V	1.23/1.15	V	1.52/1.08
V=O	0.07/-0.55	V-OH	-0.01/-0.75	O-H	0.02/-0.80
(V)O-H	0.21/-0.68	Ph_2C-O	0.34/ 0.22	Ph_2HC-O	-0.18/-0.57
Ph_2C-H-O	-0.05/0.38	V-OH-O	-0.08/-0.73	Ph_2HC-O	0.40/-0.18
Ph_2C-H-O	0.63/-0.14				
C-Y	0.001/-0.16				

Figure 10. B3LYP-optimized transitions states, Mulliken electron spin densities, and charges for H-transfer alcohol oxidation (TS_{A-B}, TS_{B-C}) and $[(salimin)VO\text{-}CHPh_2]^-$ homolysis, TS_{F-G}.

activation barrier for the associative alcoholate H-transfer pathway (35.4 kcal) relative to the sequential C−H then O−H transfer pathway (32.6 kcal) predicts that the latter would be the primary operative process for alcohol oxidation by **1**. Finally, numerous attempts to locate a TS for concerted O−H/C−H transfer from alcohol to **1** (pathway 3) to directly give benzophenone and dihydroxo complex **C** were unsuccessful, suggesting that this process has a higher energy barrier.

The post-oxidation pathway leading to the alcohol reductive coupling was considered to proceed from the reduced LV(III) aquo species **D** (Figure 9). A slightly endergonic dissociative substitution of H_2O from **D** by Ph_2CHOH via $[(salimin)VO]^-$ **E** leads to hydroxo/alkoxo species **F**. A C−O homolytic scission from **F** is exoergic to give the benzhydryl radical + V(IV) species **G** via TS_{F-G} with a ΔG_{act} value of only 20.0 kcal versus a calculated dissociation energy of approximately 80 kcal for C−O homolysis in Ph_2CH−OH.[34] From **G**, association of Ph_2CHOH and dehydration afford alkoxo complex **H**. The individual steps from **G** to **H** are not shown, but being mildly exoergic overall with proton transfers involved, they are not likely to have a high barrier. An H-atom transfer reaction of **H** with $(salimin)V(OH)_2^-$ complex **C** would produce $(salimin)\text{-}V(IV)(O)(OH)^-$ **G** and the key alkoxo-hydroxo intermediate **F**. The latter can again undergo facile C−O homolysis to give the benzhydryl radical and hydroxo-oxyl species **G**. Dimer formation via benzyhydryl radical recombination is highly exoergic and **G** can undergo H-transfer disproportionation to give starting $(salimin)VO_2^-$ (**1** = **A**) and $(salimin)V(OH)_2^-$ (**C**).

The calculated structures of the H-transfer and C−O cleavage TSs and their Mulliken atom electron spin densities for atoms in the vicinity of the bond-making/breaking in the reaction pathway are shown in Figure 10; also given are selected Mulliken partial charges for these atoms.[35] The H-transfer TSs TS_{A-B} and TS_{B-C} for alcohol oxidation exhibit considerable radical spin density at the Ph_2C, H···O, and −V atoms, showing significantly delocalized radicaloid character. The charge distribution in the TSs is considered only qualitatively significant,[36] but in the C−H transfer TS TS_{A-B}, both radical and positive charge are developed at the benzylic carbon and negative charge (and radical character) at the ligand carbon para to the salimin O−V. These features qualitatively account for the substrate and catalyst substituent effects on the rate of alcohol oxidation, that is, for the alcohols, X-BnOH, electron-donating or radical stabilizing X-groups accelerate their oxidation and for $(Y\text{-}salimin)VO_2^-$, an electron-withdrawing group accelerates its reduction.

In the TS for VO···$CHPh_2$ bond cleavage, TS_{F-G}, substantial spin density is similarly developing at the atoms of the C−O−V atom linkage. Hence, each of these bond transformations has considerable radical character and the relatively modest barriers for each of them reflect the ability of the (salimin)VO and benzhydryl fragments to distribute the electron spin density and electronic charge. To assess the electronic effects of ligand substituents on the facility of $(Y\text{-}salimin)VOH(O\text{-}CHPh_2)^-$ (**F**) C−O bond homolysis, the TSs and corresponding activation energies, E_{act}, were calculated for Y = H, OMe and NO_2. The TS structures for all three are very similar in geometry and bond metrics (Supporting Information). The activation energies, listed in Table 4, differ only by about 2 kcal

Table 4. B3LYP-Calculated Activation Energies for the C−O Homolysis of $(Y\text{-}Salimin)VOH(O\text{-}CHPh_2)^-$ (F)

substituent Y	E_{act} (kcal/mol)[a]
NO_2 (**1b**)	26.8
H (**1a**)	25.9
OMe (**1c**)	25.0

[a]Electronic energy; structures optimized with B3LYP (gas phase, 0 K).

and follow the order Y = NO_2 (**1b**) > H (**1a**) > OMe (**1c**), that is, the rate of VO···$CHPh_2$ cleavage is predicted to be **1c** > **1a** > **1b**. This ordering is explicable in that the C−O homolysis involves partial oxidation of (electron removal from) the (Y-salimin)V(OH)O fragment, which would be facilitated by an electron-donating substituent on the salimin ligand, for example, Y = OMe. The greater reactivity of $(MeO\text{-}salimin)VOH(O\text{-}CHPh_2)^-$ (F_{OMe}) agrees with the experimental estimate for the rates of reductive coupling of benzhydrol catalyzed by **1a−c** (Table 2). The negligible difference between the reductive coupling rates for Y = H and NO_2

DOI: 10.1021/acs.inorgchem.8b02968
Inorg. Chem. XXXX, XXX, XXX−XXX

may be the result of the inherent experimental error caused by the competing oxidation reaction, whose rate is affected in the opposite trend by the Y substituent. Finally, we note that the susceptibility of the V(III)-alkoxide **F** to C−O homolysis is comparable to that of $(PPh_3)OIRe(III)-O\cdots R$ cleavage implicated in the Re-catalyzed reductive coupling of activated alcohols with PPh_3 as the reductant.[13]

6. SUMMARY/CONCLUSIONS

Mechanistic probes of the oxovanadium-catalyzed Ox−RC of alcohols have revealed the following: (1) carbon free radicals are reaction intermediates as evidenced by H-abstraction trapping by fluorene. (2) Electronic substituent effects on the relative rates of X-BnOH and (Y-salimin)VO_2^- on the oxidation stage suggest developing radical and positive charge character on the benzyl unit and radical and negative charge development of the LVO unit in the oxidation. (3) DFT computational modeling of the reaction supports a ping-pong catalytic pathway beginning with alcohol oxidation by LVO_2^-, preferably by stepwise C−H then O−H atom transfers to LVO_2^-, affording the carbonyl product and the reduced $LV(III)(OH)_2$. Condensation of the latter with the alcohol would give $LV(III)(OR)OH^-$ (**F**), which undergoes homolysis of the R−OV bond to produce $LV(IV)OH(O)^-$ and the alkyl radical. The C-radical can then dimerize (or H-atom abstract) and the $LV(IV)OH(O)^-$ species disproportionate to regenerate the catalyst species LVO_2^- and $LV(OH)_2^-$.

Comparison of the calculated and experimentally supported mechanistic pathway for the oxovanadium-catalyzed Ox−RC to the reductive coupling pathway promoted by PPh_3/$ReIO_2(PPh_3)_2$ shows important similarities with at least one important difference. Both types of reactions appear to operate by turnover-limiting homolysis of a reduced metal-alkoxide species to generate carbon-centered free radicals. However, the V-catalyzed reaction apparently generates the reduced metal-alkoxide by oxidation of the substrate alcohol (PPh_3 is unchanged when present), whereas in the Re system, PPh_3 is the more effective reductant. The capability to generate C-centered radicals from alcohols, the most available of singly oxidized carbon feedstocks, holds great promise as a means of C−C bond formation, a focus of our future investigations.

7. EXPERIMENTAL SECTION

7.1. General Methods and Materials. All reactants and materials were obtained commercially and used without further modification; all solvents used were ACS grade. ^{1}H NMR spectra were obtained at 400 or 500 MHz. NMR data were analyzed using instrument's MestReNova software. IR spectra were obtained using Shimadzu IRAffinity-1 and processed using IRSolution software. Electrochemical experiments were performed using a CHI832 electrochemical analyzer. The data obtained were analyzed with the HP 8452A resident software package. UV−vis spectra were obtained with a diode array spectrophotometer and processed with the instruments software package. Tetrabutylammonium metavanadate ($(Bu)_4N^+[VO_3]^-$) was prepared according to a reported method except for our use of a 2:1 molar ratio of Bu_4NOH to V_2O_5.[37]

7.2. Preparation of SaliminH$_2$ Ligands. Equimolar amounts of 2-aminophenol (6.0 mmol) and the substituted salicylaldehyde of choice (6.0 mmol) were dissolved in THF and stirred overnight, leading to the solution changing from light yellow to orange-red. Hexane was then added to the reaction solution and the mixture was left in the freezer to further promote precipitation. Filtration then provided the substituted salimine ligands as yellow to orange solids, which were spectroscopically pure and used directly for complexation.

7.2.1. SaliminH$_2$. Upon addition of the salicylaldehyde to the solution containing aminophenol, the solution changed from light yellow to orange. Workup as above gave a 65% yield of an orange solid. ^{1}H NMR (400 MHz, $CDCl_3$): δ/ppm 12.24 (s, 1H), 8.69 (s, 1H), 7.46−7.39 (m, 2H), 7.25−7.19 (m, 1H), 7.17−7.13 (m, 1H), 7.07−6.94 (m, 1H), 5.75 (s, 1H). IR $\tilde{\nu}$/cm^{-1}: 3050 (w, C−H), 1620 (s, C═N), 1280 (s, C−N), 1150 (s, C−O), 750 (s, C−H).

7.2.2. 4-NO$_2$-SaliminH$_2$. After the addition of the salicylaldehyde to the solution containing aminophenol, the reaction solution turned from yellow to a deep red-orange. Workup gave an 87% yield of an orange-brown solid. ^{1}H NMR (500 MHz, DMSO): δ/ppm 10.37 (b, 1H), 9.30 (s, 1H), 8.62−8.59 (d, J = 3.0 Hz, 1H), 8.16 (dd, J = 9.4, 3.0 Hz, 1H), 7.58 (dd, J = 8.1, 1.5 Hz, 1H), 7.24−7.19 (m, 1H), 7.02 (dd, J = 8.2, 1.3 Hz, 1H), 6.98−6.93 (m, 1H), 6.90 (d, J = 9.4 Hz, 1H). IR $\tilde{\nu}$/cm^{-1}: 3050 (w, C−H), 1605 (s, C═N), 1520 (s, N−O), 1325 (s, N−O), 750 (s, C−H).

7.2.3. 4-MeO-SaliminH$_2$. Upon addition of 4-methoxy-salicylaldehyde to the solution containing aminophenol, the solution changed from yellow to orange. The precipitation with hexane gave a 94% yield of a red solid. ^{1}H NMR (400 MHz, $CDCl_3$): δ/ppm 11.80 (b, 1H), 8.65 (s, 1H), 7.25−7.19 (m, 1H), 7.17−7.13 (m, 1H), 7.06−6.91 (m, 5H), 5.79 (b, 1H), 3.82 (s, 3H). IR $\tilde{\nu}$/cm^{-1}: 3000 (w, C−H), 1640 (s, C═N), 1250 (s, C−N), 1150 (s, C−O), 750 (s, C−H).

7.3. Preparation of $(Bu)_4N^+[(Y\text{-Salimin})VO_2]^-$ Complexes. Tetrabutylammonium metavanadate (3.0 mmol) and the saliminH$_2$ ligand (3.0 mmol) were added to a round-bottom flask containing 20 mL of dry THF. The solution changed from orange-red to black while stirring overnight. After the reaction was complete, hexane was added to the reaction mixture to promote precipitation; then, the mixture was left in the freezer for 2 h. The mixture was then filtered, giving a yellow or brown solid that was dried under high vacuum.

*7.3.1. Bu$_4$N[(Salimin)VO$_2$] (**1a**).* Addition of the metavanadate salt to the ligand solution causes the color to change from orange to black. The addition of hexane causes the precipitation of a yellow solid. The yield was 79%. ^{1}H NMR (400 MHz, $CDCl_3$): δ/ppm 9.02 (s, 1H), 7.54 (d, J = 8.1 Hz, 1H), 7.46 (d, J = 7.8 Hz, 1H), 7.33 (t, J = 7.8 Hz, 1H), 7.09 (t, J = 7.6 Hz, 1H), 7.01 (d, J = 8.5 Hz, 1H), 6.84−6.76 (m, 2H), 6.70 (t, J = 7.6 Hz, 1H), 3.56 (bm, 8H), 1.72 (bm, 8H), 1.44 (bm, 8H), 0.96 (t, J = 7.0 Hz, 12H). ^{51}V NMR (105.08 MHz, relative to $OVCl_3$; $CDCl_3$): δ −524.0. IR $\tilde{\nu}$/cm^{-1}: 3000 (m, C−H), 1600 (s, C═N), 1290 (s, C−N), 920 (s, VO_2 sym), 840 (m, VO_2 asym). Negative ion ESI-MS: 293.9973 (m/z), calcd 293.9971. UV−vis (CH_2Cl_2) λ (nm) ε (M^{-1} cm^{-1}): 236 (1.3×10^4), 280 (8.6×10^3), 426 (5.7×10^3).

*7.3.2. Bu$_4$N[(NO$_2$-Salimin)VO$_2$] (**1b**).* Combination of the both metavanadate salt and the nitro-ligand in solution formed an orange solution, which quickly turned black. Precipitation gave a brown solid in 68% yield. ^{1}H NMR (400 MHz, DMSO): δ/ppm 9.54 (s, 1H), 8.74 (d, J = 3.0 Hz, 1H), 8.18 (dd, J = 9.3, 1.9 Hz, 1H), 7.79 (d, J = 8.1 Hz, 1H), 7.12 (t, J = 7.6 Hz, 1H), 6.91 (d, J = 9.3 Hz, 1H), 6.75−6.67 (m, 2H), 3.14 (bm, 8H), 1.55 (bm, 8H), 1.30 (bm, 8H), 0.92 (bt, J = 7.3 Hz, 12H). ^{51}V NMR (105.08 MHz, relative to $OVCl_3$; $CDCl_3$): δ −524.4. IR $\tilde{\nu}$/cm^{-1}: 3000 (m, C−H), 1600 (s, C═N), 1560 (m, N−O), 1350 (s, N−O), 900 (s, VO_2 sym), 850 (m, VO_2 asym). Negative ion ESI-MS: 338.9825 (m/z), calcd 338.9822. UV−vis (CH_2Cl_2) λ (nm) ε (M^{-1} cm^{-1}): 240 (2.1×10^4), 318 (1.5×10^4), 344 (1.5×10^4), 445 (8.9×10^3).

*7.3.3. Bu$_4$N[(MeO-Salimin)VO$_2$] (**1c**).* Upon addition of the metavanadate salt to the ligand solution, the solution turns from a deep red to black. After being left overnight, the reaction mixture contained a small amount of an orange-yellow precipitate. Workup as above gave an 85% yield of a yellow solid. ^{1}H NMR (400 MHz, $CDCl_3$): δ/ppm 8.99 (s, 1H), 7.54 (d, J = 8.2 Hz, 1H), 7.09 (t, J = 7.7 Hz, 1H), 7.0 (m, 2H), 6.93 (d, J = 2.9 Hz, 1H), 6.83 (d, J = 8.2 Hz, 1H), 3.81 (s, 3H), 3.56 (b, 8H), 1.71 (b, 8H), 1.44 (b, 8H), 0.97 (bt, J = 6.8 Hz, 12H). ^{51}V NMR (105.08 MHz, relative to $OVCl_3$; $CDCl_3$): δ −520.9. IR $\tilde{\nu}$/cm^{-1}: 3000 (m, C−H), 1600 (s, C═N), 1320 (s, C−N), 920 (s, VO_2 sym), 840 (m, VO_2 asym). Negative ion ESI-MS: 324.0082 (m/z), calcd 324.0077. UV−vis (CH_2Cl_2) λ (nm), ε (M^{-1} cm^{-1}): 236 (2.6×10^4), 280 (1.8×10^4), 446 (1.13×10^4).

DOI: 10.1021/acs.inorgchem.8b02968
Inorg. Chem. XXXX, XXX, XXX−XXX

7.4. Determination of k_{rel} for Reactions of Substituted Benzyl Alcohols Catalyzed by $Bu_4N(Salimin)VO_2$ (1). In a typical experiment, the catalyst (0.054 g, 0.100 mmol) was placed in a high-pressure Ace glass tube, along with benzyl alcohol (0.108 g, 1.00 mmol), 4-methoxybenzyl alcohol (0.138 g, 1.00 mmol), and benzene (5 mL). The tube was purged with nitrogen gas, then sealed, and heated to 150 °C for 24 h. The ratios of unreacted alcohols and product aldehydes were determined by H-NMR integration.

7.5. Kinetics of the Benzhydrol Ox−RC with Bu_4N [Y-LVO_2] (1a−c). Benzhydrol (0.184 g, 1.00 mmol) and 10 mol % (0.10 mmol) of Bu_4N[(Y-salimin)VO_2] (**1a**, **1b**, or **1c**) were added to a thick-walled Ace glass reactor tube. A measured amount of hexamethylbenzene (0.012 g, 0.074 mmol) was added as an internal standard followed by 5 mL of benzene. The reaction solution was then purged by bubbling N_2 through the solution for 1−2 min. The reactor tube was sealed with a Teflon cap with a stainless-steel sampling apparatus attached to it. Once the reactor was sealed, the system was heated to 150 °C in a silicon oil bath.

To determine the rate of production of the oxidation product, aliquots were taken every 3 h, starting 3 h after the reactor was initially placed in the oil bath. Aliquots were obtained by first withdrawing and rejecting approximately 100 μL of the reaction solution through the sampling apparatus and then collecting 200 μL of the reaction solution. The aliquot was then concentrated in vacuo and the residue was dissolved in 500 μL of $CDCl_3$. A ^{1}H NMR spectrum was obtained and processed. Yields at each time were obtained by integrating the ortho proton signal of benzophenone and the benzylic protons of 1,1,2,2-tetraphenylethane with respect to the singlet from hexamethylbenzene. The rate of consumption of the starting alcohol was monitored in the same manner as above, utilizing the benzylic proton. Concentration/time data are given in the Supporting Information.

7.6. Electrochemical Analysis. Each vanadium complex (0.02 mmol, 4 mM) was combined with Bu_4NPF_6 (0.5 mmol, 100 mM) and 5 mL of distilled dichloromethane in a 20 mL scintillation vial. The solution was then purged by bubbling nitrogen gas through it for 1−2 min. The electrodes used were platinum and glassy carbon working electrodes, a platinum counter electrode, and a Ag/AgCl pseudo-reference electrode. For CV, the potential wave swept from a positive potential to a negative potential. The scan rate used was 0.1 V/s.

7.7. Preparation of Homo- and Hetero Benzhydryl/Fluorenyl Dimers. In a sealable pressure tube, fluorene (0.165 g, 0.993 mmol), benzhydrol (0.223 g, 1.21 mmol), potassium hydroxide (0.081 g, 1.45 mmol), and benzophenone (0.019 g, 0.105 mmol) were placed along with toluene (1 mL). After sealing, the contents were heated at 170 °C for 24 h, and the crude mixture is filtered through SiO_2, giving a colorless mixture of products (0.238 g).[38]

7.8. Benzhydrol Ox−RC Reaction in the Presence of Fluorene. Benzhydrol (0.185 g, 1.00 mmol), catalyst **1a** (0.055 g, 0.104 mmol), fluorene (0.166 g, 1.00 mmol), and benzene (5 mL) were added to a thick-walled glass pressure tube. The tube was purged with nitrogen, sealed, and heated at 150 °C for 24 h. After cooling, the product mixture was analyzed by H NMR and GC−MS, including comparison with the spectra of authentic samples.

7.9. Procedure for Alcohol Coordination Studies. In an NMR tube, the complex **1a** (20 mg, 0.0037 mmol) was combined with benzhydrol (6.0 mg, 0.0033 mmol) and benzene-d_6. H-NMR spectra were taken 3 h later, as well as 4 days later. In another NMR tube experiment, the compound **1b** (12 mg, 0.022 mmol) was combined with benzhydrol (0.007 g, 0.039 mmol) and benzene-d_6. The tube was heated to 50 °C for 5 min until the catalyst dissolved and then NMR spectra were recorded.

7.10. Computational Studies. *7.10.1. General methods.* The B3LYP[28] and M06[29] methods resident in Gaussian 09[S1] were used to determine the energy-minimized structures, vibrational frequencies, and electronic energies. For the B3LYP optimizations, the 6-31G(d) basis set was used for H, C, O, N atoms and LANL2DZ for V. For single-point energy (M06) calculations, the basis sets were 6-311++G(d,p) for H, C, O, and N and SDD for V, and the SMD solvent continuum method[30] was included for modeling the species in the experimental reaction medium (benzene). The Gibbs free energies and enthalpies include zero-point vibrational energies and thermal corrections at 298 K. TSs were approached by mod-redundant scans and characterized by single imaginary frequencies with displacement along the reaction coordinate. Energy values and Cartesian (*x*,*y*,*z*) coordinates for each of the species are provided in the Supporting Information.

■ ASSOCIATED CONTENT

Ⓢ Supporting Information

The Supporting Information is available free of charge on the ACS Publications website at DOI: 10.1021/acs.inorgchem.8b02968.

Characterization data for $(Bu_4N)(salimin)VO_2$ (**1a−c**), kinetics data, DFT-calculated energies, and Cartesian coordinates for the species in the putative reaction pathway (PDF)

Energy values and Cartesian (*x*,*y*,*z*) coordinates of all of the molecules reported in this study (XYZ)

■ AUTHOR INFORMATION

Corresponding Author

*E-mail: knicholas@ou.edu.

ORCID

Kenneth M. Nicholas: 0000-0002-5180-1671

Notes

The authors declare no competing financial interest.

■ ACKNOWLEDGMENTS

K.M.N. thanks the National Science Foundation (CHE1566213) for support. We also acknowledge helpful discussions with Drs. Daniel Glatzhofer (University of Oklahoma) and Peng Liu (University of Pittsburgh). DFT calculations were performed at the OU Supercomputing Center for Education and Research (OSCER).

■ REFERENCES

(1) (a) *Topics in Current Chemistry: Selective Catalysis for Renewable Feedstocks and Chemicals*; Nicholas, K. M., Ed.; Springer International Publishing, 2014; Vol. 353. (b) Wang, L.; Xiao, F. S. *Nanoporous Catalysts for Biomass Conversion*; Xiao, F. S., Wang, L., Eds.; John Wiley & Sons: Hoboken, 2015; Vol. 17. (c) Chheda, J. N.; Huber, G. W.; Dumesic, J. A. Liquid-Phase Catalytic Processing of Biomass-Derived Oxygenated Hydrocarbons to Fuels and Chemicals. *Angew. Chem., Int. Ed.* **2007**, *46*, 7164−7183.

(2) Bhaumik, P.; Dhepe, P. L. Chapter 1. Conversion of Biomass into Sugars. *Green Chem. Ser.* **2016**, *44*, 1−53.

(3) (a) Larson, G. L.; Fry, J. L. *Ionic and Organometallic-Catalyzed Organosilane Reductions*; John Wiley & Sons: Hoboken, 2009. (b) McLaughlin, M. P.; Adduci, L. L.; Becker, J. J.; Gagné, M. R. Iridium-Catalyzed Hydrosilylative Reduction of Glucose to Hexane-(S). *J. Am. Chem. Soc.* **2013**, *135*, 1225−1227. (c) Yasuda, M.; Onishi, Y.; Ueba, M.; Miyai, T.; Baba, A. Direct Reduction of Alcohols: Highly Chemoselective Reducing System for Secondary or Tertiary Alcohols Using Chlorodiphenylsilane with a Catalytic Amount of Indium Trichloride. *J. Org. Chem.* **2001**, *66*, 7741−7744. (d) Mayr, H.; Dogan, B. Selectivities in Ionic Reductions of Alcohols and Ketones with Triethylsilane/Trifluoroacetic Acid. *Tetrahedron Lett.* **1997**, *38*, 1013−1016. (e) Hong, Y.-K.; Lee, D.-W.; Eom, H.-J.; Lee, K.-Y. The catalytic activity of Pd/WOx/γ-Al2O3 for hydrodeoxygenation of guaiacol. *Appl. Catal., B* **2014**, *150−151*, 438−445. (f) de Souza, P. M.; Rabelo-Neto, R. C.; Borges, L. E. P.; Jacobs, G.; Davis, B. H.; Sooknoi, T.; Resasco, D. E.; Noronha, F. B. Role of Keto Intermediates in the Hydrodeoxygenation of Phenol over Pd on Oxophilic Supports. *ACS Catal.* **2015**, *5*, 1318−1329. (g) Martin, A.;

DOI: 10.1021/acs.inorgchem.8b02968
Inorg. Chem. XXXX, XXX, XXX−XXX

Armbruster, U.; Gandarias, I.; Arias, P. L. Glycerol hydrogenolysis into propanediols using in situ generated hydrogen - A critical review. *Eur. J. Lipid Sci. Technol.* **2012**, *115*, 9−27. (h) Tomishige, K.; Nakagawa, Y.; Tamura, M. Selective Hydrogenolysis of C-O Bonds Using the Interaction of the Catalyst Surface and OH Groups. In *Topics in Current Chemistry: Selective Catalysis for Renewable Feedstocks and Chemicals*; Nicholas, K. M., Ed.; Springer International Publishing, 2014; Vol. *353*, pp 127−162. (i) Murru, S.; Nicholas, K. M.; Srivastava, R. S. Ruthenium (II) Sulfoxides-Catalyzed Hydrogenolysis of Glycols and Epoxides. *J. Mol. Catal. A: Chem.* **2012**, *363*−*364*, 460−464. (j) Schlaf, M.; Ghosh, P.; Fagan, P. J.; Hauptman, E.; Bullock, R. M. Catalytic Deoxygenation of 1,2-Propanediol to Given-Propanol. *Adv. Synth. Catal.* **2009**, *351*, 789−800.

(4) (a) Petersen, A. R.; Fristrup, P. New Motifs in Deoxydehydration: Beyond the Realms of Rhenium. *Chem.—Eur. J.* **2017**, *23*, 10235−10243. (b) Mao, G.; Jia, B.; Wang, C. Recent Progress in Re-Catalyzed Dehydroxylation Reactions. *Chin. J. Org. Chem.* **2015**, *35*, 284−293. (c) Dethlefsen, J. R.; Fristrup, P. Rhenium-Catalyzed Deoxydehydration of Diols and Polyols. *ChemSusChem* **2014**, *8*, 767−775. (d) Boucher-Jacobs, C.; Nicholas, K. M. Deoxydehydration of Polyols. In *Topics in Current Chemistry: Selective Catalysis for Renewable Feedstocks and Chemicals*; Nicholas, K. M., Ed.; Springer International Publishing, 2014; Vol. *353*, pp 163−184.

(5) (a) Cook, G. K.; Andrews, M. A. Toward Nonoxidative Routes to Oxygenated Organics: Stereospecific Deoxydehydration of Diols and Polyols to Alkenes and Allylic Alcohols Catalyzed by the Metal Oxo Complex (C5Me5)ReO3. *J. Am. Chem. Soc.* **1996**, *118*, 9448−9449. (b) Ziegler, J. E.; Zdilla, M. J.; Evans, A. J.; Abu-Omar, M. M. H2-Driven Deoxygenation of Epoxides and Diols to Alkenes Catalyzed by Methyltrioxorhenium. *Inorg. Chem.* **2009**, *48*, 9998−10000. (c) Arceo, E.; Ellman, J. A.; Bergman, R. G. Rhenium-Catalyzed Didehydroxylation of Vicinal Dials to Alkenes Using a Simple Alcohol as a Reducing Agent. *J. Am. Chem. Soc.* **2010**, *132*, 11408−11409. (d) Vkuturi, S.; Chapman, G.; Ahmad, I.; Nicholas, K. M. Rhenium-Catalyzed Deoxydehydration of Glycols by Sulfite. *Inorg. Chem.* **2010**, *49*, 4744−4746.

(6) (a) Chapman, G.; Nicholas, K. M. Vanadium-Catalyzed Deoxydehydration of Glycols. *Chem. Commun.* **2013**, *49*, 8199−8201. (b) Gopaladasu, T. V.; Nicholas, K. M. Carbon Monoxide (CO)- and Hydrogen-Driven, Vanadium-Catalyzed Deoxydehydration of Glycols. *ACS Catal.* **2016**, *6*, 1901−1904.

(7) Dethlefsen, J. R.; Lupp, D.; Teshome, A.; Nielsen, L. B.; Fristrup, P. Molybdenum-Catalyzed Conversion of Diols and Biomass-Derived Polyols to Alkenes Using Isopropyl Alcohol as Reductant and Solvent. *ACS Catal.* **2015**, *5*, 3638−3647.

(8) Kasner, G. R.; Boucher-Jacobs, C.; Michael McClain, J.; Nicholas, K. M. Oxo-Rhenium Catalyzed Reductive Coupling and Deoxygenation of Alcohols. *Chem. Commun.* **2016**, *52*, 7257−7260.

(9) (a) van Tamelen, E. E.; Schwartz, M. A. Reductive Coupling of Alcohols to Hydrocarbons. *J. Am. Chem. Soc.* **1965**, *87*, 3277−3278. (b) McMurry, J. E.; Silvestri, M. Simplified method for the titanium(II)-induced coupling of allylic and benzylic alcohols. *J. Org. Chem.* **1975**, *40*, 2687−2688. (c) Kulinkovich, O. G.; Isakov, V. E. The Head-to-Head Reductive Coupling of Homoallylic Alcohols Promoted by Titanium (II)-Olefin Complexes. *Synlett* **2003**, 0967−0970. (d) Karunakar, G. V.; Periasamy, M. A Simple Method for the Conversion of Propargyl Alcohols to Symmetrical 1,5-Diynes Using Low Valent Titanium Reagents. *Tetrahedron Lett.* **2006**, *47*, 3549−3552.

(10) Nishino, T.; Nishiyama, Y.; Sonoda, N. Lanthanum Metal-Assisted Deoxygenative Coupling of Alcohols. *Tetrahedron Lett.* **2002**, *43*, 3689−3691.

(11) Nishino, T.; Nishiyama, Y.; Sonoda, N. Deoxygenative Dimerization of Benzylic and Allylic Alcohols, and Their Ethers and Esters Using Lanthanum Metal and Chlorotrimethylsilane in the Presence of a Catalytic Amount of Iodine and Copper(I) Iodide. *Bull. Chem. Soc. Jpn.* **2003**, *76*, 635−641.

(12) (a) Gabriëls, D.; Hernández, W. Y.; Sels, B.; Van Der Voort, P.; Verberckmoes, A. Review of Catalytic Systems and Thermodynamics for the Guerbet Condensation Reaction and Challenges for Biomass Valorization. *Catal. Sci. Technol.* **2015**, *5*, 3876−3902. (b) Aitchison, H.; Wingad, R. L.; Wass, D. F. Homogeneous Ethanol to Butanol Catalysis—Guerbet Renewed. *ACS Catal.* **2016**, *6*, 7125−7132. (c) Kozlowski, J. T.; Davis, R. J. Heterogeneous Catalysts for the Guerbet Coupling of Alcohols. *ACS Catal.* **2013**, *3*, 1588−1600.

(13) Boucher-Jacobs, C.; Liu, P.; Nicholas, K. M. Mechanistic Insights into the ReIO2(PPh3)2-Promoted Reductive Coupling of Alcohols. *Organometallics* **2018**, *37*, 2468−2480.

(14) Steffensmeier, E.; Nicholas, K. M. Oxidation-reductive Coupling of Alcohols Catalyzed by Oxo-Vanadium Complexes. *Chem. Commun.* **2018**, *54*, 790−793.

(15) Mullins, R. J.; Vedernikov, A.; Viswanathan, R. Competition Experiments as a Means of Evaluating Linear Free Energy Relationships. An Experiment for the Advanced Undergraduate Organic Chemistry Lab. *J. Chem. Educ.* **2004**, *81*, 1357.

(16) (a) Hansch, C.; Leo, A.; Taft, R. W. A Survey of Hammett Substituent Constants and Resonance and Field Parameters. *Chem. Rev.* **1991**, *91*, 165−195. (b) Hammett, L. P. The Effect of Structure upon the Reactions of Organic Compounds. Benzene Derivatives. *J. Am. Chem. Soc.* **1937**, *59*, 96−103.

(17) (a) Creary, X.; Mehrsheikh-Mohammadi, M. E.; McDonald, S. Methylenecyclopropane rearrangement as a probe for free radical substituent effects. .sigma..bul. Values for commonly encountered conjugating and organometallic groups. *J. Org. Chem.* **1987**, *52*, 3254−3263. (b) Hikawa, H.; Mori, Y.; Kikkawa, S.; Azumaya, I. A Radical Pathway for Direct Substitution of Benzyl Alcohols with Water-Soluble Copper Catalyst in Water. *Adv. Synth. Catal.* **2016**, *358*, 765−773.

(18) Rehder, D.; Polenova, T.; Bühl, M. Vanadium-51 NMR. *Annu. Rep. NMR Spectrosc.* **2007**, *62*, 49−114.

(19) (a) Cook, P. F.; Cleland, W. W. *Enzyme Kinetics and Mechanism*, 1st ed.; Garland Science: New York, 2007. (b) Shearer, J. Insight into the Structure and Mechanism of Nickel-Containing Superoxide Dismutase Derived from Peptide-Based Mimics. *Acc. Chem. Res.* **2014**, *47*, 2332−2341.

(20) (a) Galloni, P.; Conte, V.; Floris, B. A Journey into the Electrochemistry of Vanadium Compounds. *Coord. Chem. Rev.* **2015**, *301*−*302*, 240−299. (b) Asgedom, G.; Sreedhara, A.; Kivikoski, J.; Valkonen, J.; Rao, C. P. Mononuclear cis-dioxovanadium(V) anionic complexes [VO2L]-{H2L =[1 + 1] Schiff base derived from salicylaldehyde (or substituted derivatives) and 2-amino-2-methyl-propan-l-ol}: synthesis, structure, spectroscopy, electrochemistry and reactivity studies. *J. Chem. Soc., Dalton Trans.* **1995**, *14*, 2459−2466. (c) Das, C.; Adak, P.; Mondal, S.; Sekiya, R.; Kuroda, R.; Gorelsky, S. I.; Chattopadhyay, S. K. Synthesis, Characterization, X-Ray Crystal Structure, DFT Calculations, and Catalytic Properties of a Dioxidovanadium(V) Complex Derived from Oxamohydrazide and Pyridoxal: A Model Complex of Vanadate-Dependent Bromoperoxidase. *Inorg. Chem.* **2014**, *53*, 11426−11437.

(21) Taft, R. W., Jr. A Precise Correlation of Nuclear Magnetic Shielding in M- and p-Substituted Fluorobenzenes by Inductive and Resonance Parameters from Reactivity. *J. Am. Chem. Soc.* **1957**, *79*, 1045−1049.

(22) (a) Ebrahimipour, S. Y.; Abaszadeh, M.; Castro, J.; Seifi, M. Synthesis, X-Ray Crystal Structure, DFT Calculation and Catalytic Activity of Two New Oxido-Vanadium(V) Complexes Containing ONO Tridentate Schiff Bases. *Polyhedron* **2014**, *79*, 138−150. (b) Clague, M. J.; Keder, N. L.; Butler, A. Biomimics of vanadium bromoperoxidase: Vanadium(V)-Schiff base catalyzed oxidation of bromide by hydrogen peroxide. *Inorg. Chem.* **1993**, *32*, 4754−4761. (c) Hartung, J.; Drees, S.; Greb, M.; Schmidt, P.; Svoboda, I.; Fuess, H.; Murso, A.; Stalke, D. (Schiff-base)vanadium(V) Complex-Catalyzed Oxidations of Substituted Bis(homoallylic) Alcohols − Stereoselective Synthesis of Functionalized Tetrahydrofurans. *Eur. J. Org. Chem.* **2003**, 2388−2408.

(23) Ebrahimipour, S. Y.; Sheikhshoaie, I.; Kautz, A. C.; Ameri, M.; Pasban-Aliabadi, H.; Amiri Rudbari, H.; Bruno, G.; Janiak, C. Mono- and Dioxido-Vanadium(V) Complexes of a Tridentate ONO Schiff

DOI: 10.1021/acs.inorgchem.8b02968
Inorg. Chem. XXXX, XXX, XXX−XXX

Base Ligand: Synthesis, Spectral Characterization, X-Ray Crystal Structure, and Anticancer Activity. *Polyhedron* **2015**, *93*, 99−105.
(24) (a) Lyaskovskyy, V.; de Bruin, B. Redox Non-Innocent Ligands: Versatile New Tools to Control Catalytic Reactions. *ACS Catal.* **2012**, *2*, 270−279. (b) Kaim, W.; Schwederski, B. Non-innocent ligands in bioinorganic chemistry-An overview. *Coord. Chem. Rev.* **2010**, *254*, 1580−1588.
(25) (a) Geethalakshmi, K. R.; Waller, M. P.; Bühl, M. The Presumption of Innocence? A DFT-Directed Verdict on Oxidized Amavadin and Vanadium Catecholate Complexes. *Inorg. Chem.* **2007**, *46*, 11297−11307. (b) Chatterjee, P. B.; Goncharov-Zapata, O.; Quinn, L. L.; Hou, G.; Hamaed, H.; Schurko, R. W.; Polenova, T.; Crans, D. C. Characterization of Noninnocent Metal Complexes Using Solid-State NMR Spectroscopy:o-Dioxolene Vanadium Complexes. *Inorg. Chem.* **2011**, *50*, 9794−9803.
(26) (a) Akbarzadeh, T. N.; Amiri, L. O. Synthesis and Characterization of Barium-Vanadium Oxide Nanocomposite Using a Facile Thermolysis Approach. *Orient. J. Chem.* **2015**, *31*, 2247−2251. (b) Chen, C.; Bai, F.-Y.; Zhang, R.; Song, G.; Shan, H.; Xing, N.; Xing, Y.-H. Synthesis, Structure, And Catalytic Bromination of Supramolecular Oxovanadium Complexes Containing Oxalate. *J. Coord. Chem.* **2013**, *66*, 671−688. (c) Ghosh, T. Dioxovanadium(V) Complexes Incorporating Tridentate ONO Donor Hydrazone Ligands Derived from Acetylhydrazide and 2-hydroxybenzaldehyde/2-hydroxyacetophenone. Synthesis, Characterization and Reactivity. *Transition Met. Chem.* **2006**, *31*, 560−565.
(27) (a) Hanson, S. K.; Baker, R. T.; Gordon, J. C.; Scott, B. L.; Silks, L. A. P.; Thorn, D. L. Mechanism of Alcohol Oxidation by Dipicolinate Vanadium(V): Unexpected Role of Pyridine. *J. Am. Chem. Soc.* **2010**, *132*, 17804−17816. (b) Maeda, Y.; Kakiuchi, N.; Matsumura, S.; Nishimura, T.; Uemura, S. Oxovanadium Complex-Catalyzed Oxidation of Propargylic Alcohols Using Molecular Oxygen. *Tetrahedron Lett.* **2001**, *42*, 8877−8879.
(28) Becke, A. D. Density-functional thermochemistry. III. The role of exact exchange. *J. Chem. Phys.* **1993**, *98*, 5648.
(29) (a) Wang, Y.; Jin, X.; Yu, H. S.; Truhlar, D. G.; He, X. Revised M06-L Functional for Improved Accuracy on Chemical Reaction Barrier Heights, Noncovalent Interactions, and Solid-State Physics. *Proc. Natl. Acad. Sci. U.S.A.* **2017**, *114*, 8487−8492. (b) Zhao, Y.; Truhlar, D. G. The M06 suite of density functionals for main group thermochemistry, thermochemical kinetics, noncovalent interactions, excited states, and transition elements: two new functionals and systematic testing of four M06-class functionals and 12 other functionals. *Theor. Chem. Acc.* **2007**, *120*, 215−241.
(30) Marenich, A. V.; Cramer, C. J.; Truhlar, D. G. Universal Solvation Model Based on Solute Electron Density and on a Continuum Model of the Solvent Defined by the Bulk Dielectric Constant and Atomic Surface Tensions. *J. Phys. Chem. B* **2009**, *113*, 6378−6396.
(31) (a) de Vicente Poutás, L. C.; Castiñeira Reis, M.; Sanz, R.; López, C. S.; Faza, O. N. A Radical Mechanism for the Vanadium-Catalyzed Deoxydehydration of Glycols. *Inorg. Chem.* **2016**, *55*, 11372−11382. (b) Jiang, Y.-Y.; Jiang, J.-L.; Fu, Y. Mechanism of Vanadium-Catalyzed Deoxydehydration of Vicinal Diols: Spin-Crossover-Involved Processes. *Organometallics* **2016**, *35*, 3388−3396. (c) Galindo, A. DFT Studies on the Mechanism of the Vanadium-Catalyzed Deoxydehydration of Diols. *Inorg. Chem.* **2016**, *55*, 2284−2289.
(32) (a) Telser, J.; Wu, C.-C.; Chen, K.-Y.; Hsu, H.-F.; Smirnov, D.; Ozarowski, A.; Krzystek, J. Aminocarboxylate Complexes of Vanadium(III): Electronic Structure Investigation by High-Frequency and -Field Electron Paramagnetic Resonance Spectroscopy. *J. Inorg. Biochem.* **2009**, *103*, 487−495. (b) Tregenna-Piggott, P. L. W.; Carver, G. Structure and Bonding of the Vanadium(III) Hexa-Aqua Cation. 2. Manifestation of Dynamical Jahn−Teller Coupling in Axially Distorted Vanadium(III) Complexes. *Inorg. Chem.* **2004**, *43*, 8061−8071.
(33) (a) Saouma, C. T.; Mayer, J. M. Do Spin State and Spin Density Affect Hydrogen Atom Transfer Reactivity? *Chem. Sci.* **2014**, *5*, 21−31. (b) Waidmann, C. R.; Zhou, X.; Tsai, E. A.; Kaminsky, W.; Hrovat, D. A.; Borden, W. T.; Mayer, J. M. Slow Hydrogen Atom Transfer Reactions of Oxo- and Hydroxo-Vanadium Compounds: The Importance of Intrinsic Barriers. *J. Am. Chem. Soc.* **2009**, *131*, 4729−4743. (c) Dietl, N.; Schlangen, M.; Schwarz, H. Thermal Hydrogen-Atom Transfer from Methane: The Role of Radicals and Spin States in Oxo-Cluster Chemistry. *Angew. Chem., Int. Ed.* **2012**, *51*, 5544−5555. (d) Hill, C. L. Catalytic Oxygenation of Unactivated C-H Bonds. Superior Oxo Transfer Catalysts and the "Inorganic Metalloporphyrin. *Act. Funct. Alkanes* **1989**, 243−279.
(34) (a) Luo, Y.-R. *Handbook of Bond Dissociation Energies in Organic Compounds*; CRC Press: Boca Raton, 2003. (b) Li, X.-H.; Yin, G.-X.; Zhang, X.-Z. Theoretical Studies on Bond Dissociation Energies for Some Aliphatic Alcohol Compounds By Density Functional Theory and Cbs-Q Method. *J. Theor. Comput. Chem.* **2011**, *10*, 179−189.
(35) Marti, J. A New Method for Assessing Similarities among Atoms in Molecules. *Chem. Phys.* **2001**, *265*, 263−271.
(36) Grayson, M. Monopoles, Dipoles, Quadrupoles and Octopoples, a Chemist's Perspective. *Recent Res. Dev. Quantum Chem.* **2000**, *1*, 1−18.
(37) Day, V. W.; Klemperer, W. G.; Yagasakl, A. Synthesis and Structure of the New Organometallic Polyoxovanadates, $([[(C_8H_{12})Ir]_2(V_4O_{12}))^{2-}$ and $[(C_8H_{12})Ir(V_4O_{12})]_3$. *Chem. Lett.* **1990**, *19*, 1267−1270.
(38) Chen, J.; Li, Y.; Li, S.; Liu, J.; Zheng, F.; Zhang, Z.; Xu, Q. Aldehyde/Ketone-Catalyzed Highly Selective Synthesis of 9-Monoalkylated Fluorenes by Dehydrative C-Alkylation with Primary and Secondary Alcohols. *Green Chem.* **2017**, *19*, 623−628.

DOI: 10.1021/acs.inorgchem.8b02968
Inorg. Chem. XXXX, XXX, XXX−XXX